

Article

The Variation in Chemical Composition and Source Apportionment of PM_{2.5} before, during, and after COVID-19 Restrictions in Zhengzhou, China

Jinting Huang^{1,2}, Aomeng Cai^{2,3}, Weisi Wang⁴, Kuan He^{1,*}, Shuangshuang Zou² and Qingxia Ma^{2,3,*}

¹ College of Surveying and Mapping Engineering, Yellow River Conservancy Technical Institute, Kaifeng 475004, China; jenkins1204@126.com

² Key Laboratory of Geospatial Technology for the Middle and Lower Yellow River Regions, Ministry of Education, College of Geography and Environmental Science, Henan University, Kaifeng 475004, China

³ Henan Key Laboratory of Integrated Air Pollution Control and Ecological Security, Kaifeng 475004, China

⁴ Henan Ecological and Environmental Monitoring Center, Zhengzhou 450007, China

* Correspondence: hekuan@yrcti.edu.cn (K.H.); mqx@henu.edu.cn (Q.M.)

Abstract: Despite significant improvements in air quality during and after COVID-19 restrictions, haze continued to occur in Zhengzhou afterwards. This paper compares ionic compositions and sources of PM_{2.5} before (2019), during (2020), and after (2021) the restrictions to explore the reasons for the haze. The average concentration of PM_{2.5} decreased by 28.5% in 2020 and 27.9% in 2021, respectively, from 102.49 $\mu\text{g m}^{-3}$ in 2019. The concentration of secondary inorganic aerosols (SIAs) was 51.87 $\mu\text{g m}^{-3}$ in 2019, which decreased by 3.1% in 2020 and 12.8% in 2021. In contrast, the contributions of SIAs to PM_{2.5} increased from 50.61% (2019) to 68.6% (2020) and 61.2% (2021). SIAs contributed significantly to PM_{2.5} levels in 2020–2021. Despite a 22–62% decline in NO_x levels in 2020–2021, the increased O₃ caused a similar NO₃⁻ concentration (20.69–23.00 $\mu\text{g m}^{-3}$) in 2020–2021 to that (22.93 $\mu\text{g m}^{-3}$) in 2019, hindering PM_{2.5} reduction in Zhengzhou. Six PM_{2.5} sources, including secondary inorganic aerosols, industrial emissions, coal combustion, biomass burning, soil dust, and traffic emissions, were identified by the positive matrix factorization model in 2019–2021. Compared to 2019, the reduction in PM_{2.5} from the secondary aerosol source in 2020 and 2021 was small, and the contribution of secondary aerosol to PM_{2.5} increased by 13.32% in 2020 and 12.94% in 2021. In comparison, the primary emissions, including biomass burning, traffic, and dust, were reduced by 29.71% in 2020 and 27.7% in 2021. The results indicated that the secondary production did not significantly contribute to the PM_{2.5} decrease during and after the COVID-19 restrictions. Therefore, it is essential to understand the formation of secondary aerosols under high O₃ and low precursor gases to mitigate air pollution in the future.

Keywords: haze; reduced PM_{2.5} level; stable NO₃⁻ level; high O₃



Citation: Huang, J.; Cai, A.; Wang, W.; He, K.; Zou, S.; Ma, Q. The Variation in Chemical Composition and Source Apportionment of PM_{2.5} before, during, and after COVID-19 Restrictions in Zhengzhou, China. *Toxics* **2024**, *12*, 81. <https://doi.org/10.3390/toxics12010081>

Academic Editors: Chunlei Cheng and Cheng Wu

Received: 6 December 2023

Revised: 13 January 2024

Accepted: 15 January 2024

Published: 17 January 2024



Copyright: © 2024 by the authors. Licensee MDPI, Basel, Switzerland. This article is an open access article distributed under the terms and conditions of the Creative Commons Attribution (CC BY) license (<https://creativecommons.org/licenses/by/4.0/>).

1. Introduction

Despite significant improvements in air quality since strict restrictions on residential and industrial activities were implemented to prevent the spread of COVID-19 [1–6], haze formed in the North China Plain (NCP). Many studies have reported that the efficient formation of secondary aerosol species, including nitrate and sulfate, induced occurrences of haze during the restrictions [7–9]. The formation of secondary aerosol species changed significantly before, during, and after the COVID-19 restrictions, but the factors of this variation remain unclear.

Nitrate (NO₃⁻) and sulfate (SO₄²⁻) are two main species of secondary inorganic aerosols that contributed to the haze pollution [10,11]. Their precursor gases (NO_x and SO₂) are primarily produced by anthropogenic primary emissions. Due to COVID-19 restrictions,

NO_x and SO_2 concentrations have been reduced in the NCP. However, secondary pollution was enhanced in these anomalies, and they dominated the $\text{PM}_{2.5}$ level [12–14].

SO_4^{2-} is formed from SO_2 through gas, aqueous, and heterogeneous reactions like those in the aqueous phase [11,12,15–17]. Studies found that the RH of ambient air was a major factor in SO_4^{2-} conversion via heterogeneous reactions, and a high RH could enhance the heterogeneous formation of SO_4^{2-} [18–20]. NO and NO_2 are oxidized by a hydroxyl radical (OH) and O_3 to produce nitric gas (HNO_3), and then HNO_3 is aerosolized with inorganic cations [21–27]. Wang et al. (2016) found that when NO_2 levels are high, aerosol heterogeneous reactions from SO_2 and NO_2 produce SO_4^{2-} and NO_3^- . In addition, the formation reactions of SO_4^{2-} and NO_3^- are influenced by NH_3 and O_3 concentrations, relative humidity (RH), and temperature [13,24,27,28].

COVID-19 restrictions, such as reduced transportation on roads, industry, construction sites, and restaurants, influenced anthropogenic pollutant emissions [29–33]. However, the large reduction (30~70%) in NO_x and decrease (15~30%) in $\text{PM}_{2.5}$ did not eliminate the occurrence of haze [8,13,30,31,34]. Instead, O_3 levels increased by 100~200% [32,35]. Studies have attempted to elucidate why haze events occurred during COVID-19 restrictions in China. Some papers confirmed that the contribution of SIAs to $\text{PM}_{2.5}$ increased significantly in Beijing–Tianjin–Hebei and cities in northern China during restrictions, which prevented the continued decline in $\text{PM}_{2.5}$, resulting in $\text{PM}_{2.5}$ levels being higher than China's National Ambient Air Quality Standards (NAAQS, $\text{PM}_{2.5}$ of $75 \mu\text{g m}^{-3}$) [8,14,36–39]. It was reported that the enhanced contribution of sulfate and oxygenated organic aerosol inhibited further $\text{PM}_{2.5}$ reduction in Shanghai, Lanzhou, and Xi'an [7,37,38]. Recent papers revealed that efficient secondary aerosol formation might have offset the reduction in primary emissions or decreased $\text{PM}_{2.5}$ in Beijing and Hangzhou [8,9,38,40].

COVID-19 restrictions led to substantially reduced emissions of anthropogenic pollutants in big cities in the NCP. They provided an opportunity to investigate the response of air quality to reductions in air pollutants caused by human activities and the processes that caused the haze. Zhengzhou is one of the most populous cities in the southern NCP. Despite significant improvements in air quality in recent years, haze still occurs in Zhengzhou [41,42]. Restrictions were implemented in Zhengzhou (24 January to 18 February 2020) to strictly regulate human, industrial, and construction activities to stop the spread of COVID-19. As the COVID-19 pandemic is still ongoing in Zhengzhou, changes in the chemical composition and source apportionment of $\text{PM}_{2.5}$ and the reasons for these variations must be investigated in detail. This study compared the ionic composition and sources of $\text{PM}_{2.5}$ in the city during restrictions with those before and after restrictions (24 January to 18 February, 2019 and 2021). This study analyzed the changes in NO_3^- and SO_4^{2-} formation before, during, and after restrictions and explored the causes of haze.

2. Methods

2.1. Observation Site and Instruments

The observation site was at the environment monitoring supersite of Henan province in Zhengzhou (34.76°N , 113.70°E , Figure 1). This study utilized observational data from 24 January to 18 February in 2019, 2020, and 2021. The three observation periods were studied and compared: 24 January to 18 February 2020 (the restriction period in Zhengzhou); 24 January to 18 February 2019 (the comparison period before the restriction period); and 24 January to 18 February 2021 (the comparison period after the restriction).

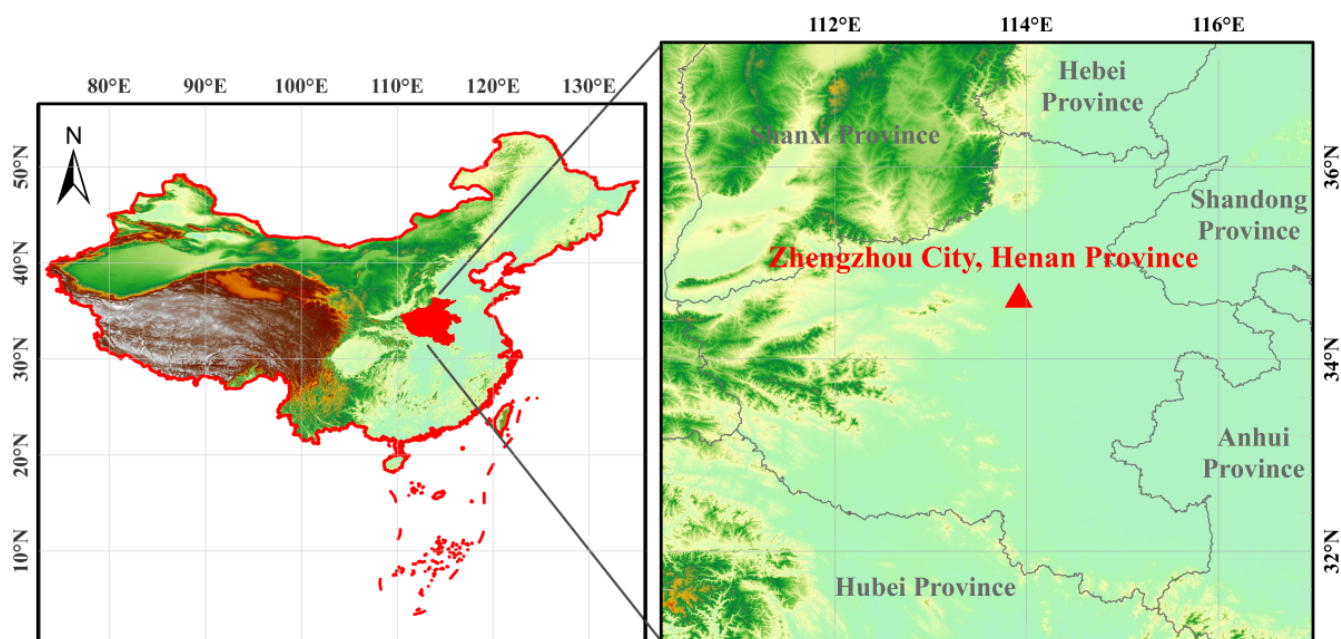


Figure 1. Location of the site (Zhengzhou) and topography in China.

The meteorological conditions (pressure, temperature, relative humidity, wind speed, and wind direction) were measured by a weather station (WS601-UMB, Luftt Instruments, Inc., Stuttgart, Germany). The concentrations of PM_{2.5}, PM₁₀, O₃, SO₂, NO_x, and CO were routinely measured through a series of pollutant detectors (5030, 5014i, 49I, 42I, 43I, 48I; Thermo Fisher Scientific, Waltham, MA, USA) at a time resolution of 5 min. A one-hour average of air pollutants and weather conditions was applied.

An online analyzer for monitoring aerosols and gases (MARGA, model ADI 2080 Applikon Analytical B. V. Corp., Petten, The Netherlands) measured the hourly mass concentrations of NH₄⁺, Na⁺, K⁺, Ca²⁺, Mg²⁺, SO₄²⁻, NO₃⁻, and Cl⁻ in PM_{2.5} at a flow rate of 16.7 L min⁻¹ [43,44]. To ensure data accuracy, the seven-point calibration curve of each species and an internal standard solution were conducted before each campaign. In addition, sampling flow calibration and cyclone cleaning were conducted to eliminate instrumental drifts. The concentrations of organic carbon (OC) and elemental carbon (EC) in PM_{2.5} were measured using a thermo-optical OC/EC analyzer (Model RT-4, Sunset Lab, Tigard, OR, USA). Elements in PM_{2.5}, including K, Ca, Zn, Cu Ni, Fe, Pb, Se, Cr, Mn, As, Co, Ti, Mo, Sc, V, Ba, Br, and Si, were quantified using an online analyzer for monitoring (AMMS-100, Focused Photonics Inc., Hangzhou, China). The formulas of major components in PM_{2.5} and the conversion rates of SO₂ to sulfate (SOR) and NO_x to nitrate (NOR) are listed in Table 1.

Table 1. Formulas and references of main components in PM_{2.5}.

Main Components	Formulas	References
Secondary inorganic aerosols (SIAs)	SO ₄ ²⁻ + NO ₃ ⁻ + NH ₄ ⁺	[27]
Primary organic aerosol (POA)	$\rho[\text{POA}] = 1.6 \times \rho[\text{EC}] \times (\rho[\text{OC}]/\rho[\text{EC}])_{\text{min}}$	[36]
Secondary organic aerosol (SOA)	$\rho[\text{SOA}] = 1.6 \times (\rho[\text{OC}] - \rho[\text{POC}])$	[43]
The conversion ratios of SO ₂ to sulfate (SOR)	$[\text{SO}_4^{2-}] / ([\text{SO}_4^{2-}] + [\text{SO}_2])$	[37]
The conversion ratios of NO _x to nitrate (NOR)	$[\text{NO}_3^-] / ([\text{NO}_3^-] + [\text{NO}] + [\text{NO}_2])$	[13]

Where $\rho[x]$ is the mass concentration of x species ($\mu\text{g m}^{-3}$). $[x]$ is the molar concentration of x species ($\mu\text{mol m}^{-3}$).

2.2. PMF Model

The origins of PM_{2.5} were analyzed using the USEPA version 5.0 positive matrix factorization (PMF) model. This model is a widely used receptor model, has high efficiency and convenience without using pollution discharge conditions, and allows additional constraints to be added into the factor profiles or contributions to reduce results' uncertainties. Input factors of the model include eight water-soluble ions (e.g., Na⁺, NH₄⁺, K⁺, Mg²⁺, Ca²⁺, NO₃⁻, SO₄²⁻, and Cl⁻) and nine target metal elements (e.g., Si, Fe, Ti, Zn, Sb, Mn, Cu, Pb, and Cr), as well as the PM_{2.5} mass concentration. In this study, five source types were tested in the analysis. More details about PMF running and result diagnosis are in the Supplementary Materials.

3. Results

3.1. Weather Conditions and Air Pollutants

Figure 2 illustrates the variations in wind direction (Wd), wind speed (Ws), relative humidity (RH), temperature (T), and air pollutant concentrations (PM₁₀, PM_{2.5}, CO, O₃, NO₂, NO, and SO₂). The average wind speed (Ws) was $1.67 \pm 1.01 \text{ m s}^{-1}$ during the 2020 COVID-19 restrictions, $1.79 \pm 1.06 \text{ m s}^{-1}$ in 2019, and $1.67 \pm 1.00 \text{ m s}^{-1}$ in 2021. The results indicate that the wind was weak in all periods. The average temperature (T) was $3.20 \pm 4.17 \text{ }^\circ\text{C}$ in 2019 and increased to $6.72 \pm 4.41 \text{ }^\circ\text{C}$ in 2020 and $9.81 \pm 3.99 \text{ }^\circ\text{C}$ in 2021. The average RH was 60–61% during the 2020 COVID-19 restrictions and in 2019, but 46% in 2021.

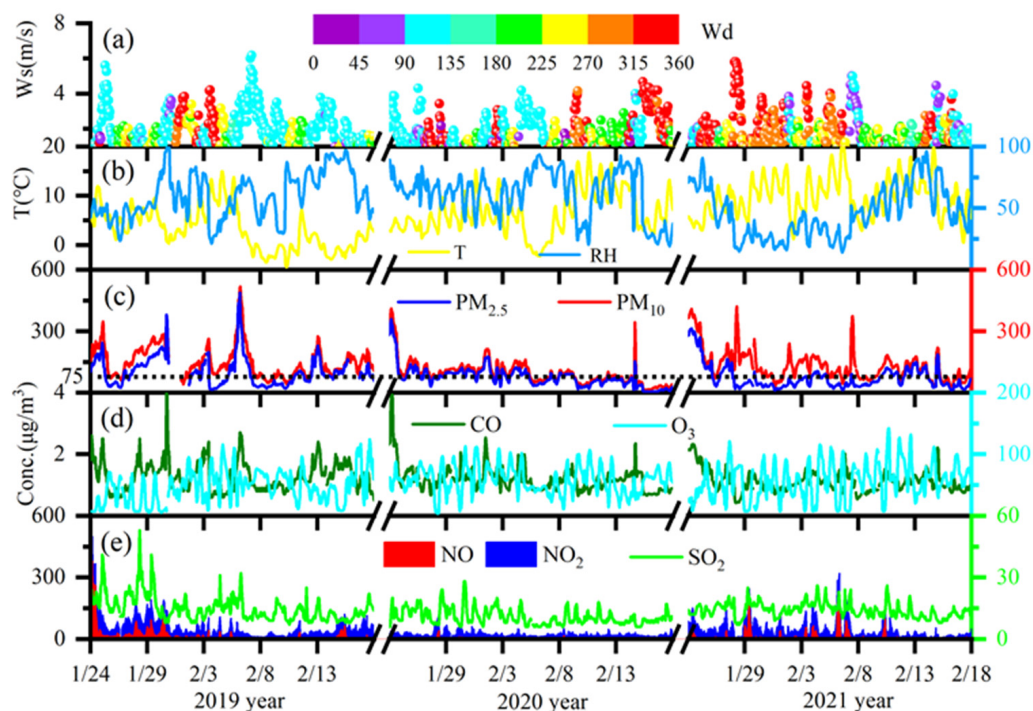


Figure 2. Evolution of meteorological conditions (a,b), particulate matter (PM₁₀ and PM_{2.5}) (c), and gaseous pollutants (NO, NO₂, SO₂, CO, and O₃) (d,e) in 2019, 2020, and 2021.

The average concentrations of PM₁₀ and PM_{2.5} were 148.49 and 102.49 $\mu\text{g m}^{-3}$ in 2019, and they decreased by 38% and 29% in 2020 and 11% and 28% in 2021 (Figure 3), respectively, resulting in a significant decline in particles in 2020 and 2021. However, the episodic haze formed with a PM_{2.5} value of more than 75 $\mu\text{g m}^{-3}$ in 2020 and 2021. At the same time, the average concentrations of NO₂, NO, SO₂, and CO in 2019 were $44.45 \pm 25.74 \mu\text{g m}^{-3}$, $24.89 \pm 49.49 \mu\text{g m}^{-3}$, $14.90 \pm 6.11 \mu\text{g m}^{-3}$, and $1.25 \pm 0.49 \text{ mg m}^{-3}$, respectively. NO₂, NO, SO₂, and CO concentrations decreased by approximately 51%, 90%, 28%, and 6% in 2020, respectively. In addition, NO₂, NO, SO₂, and CO concentrations

in 2021 were lower by 18%, 58%, 7%, and 11% than in 2019. NO₂, NO, SO₂, and CO are mainly emitted by primary emissions. The reductions in NO₂, NO, SO₂, and CO levels indicated that primary emissions may have decreased in 2020 and 2021. In contrast, the concentration of O₃ increased from 46.70 µg m⁻³ in 2019 to 58.24 µg m⁻³ in 2020 and 56.75 µg m⁻³ in 2021. The increased O₃ concentration was found in many cities (e.g., Xi'an, Shanghai, Beijing, and Hangzhou) [7,9,39].

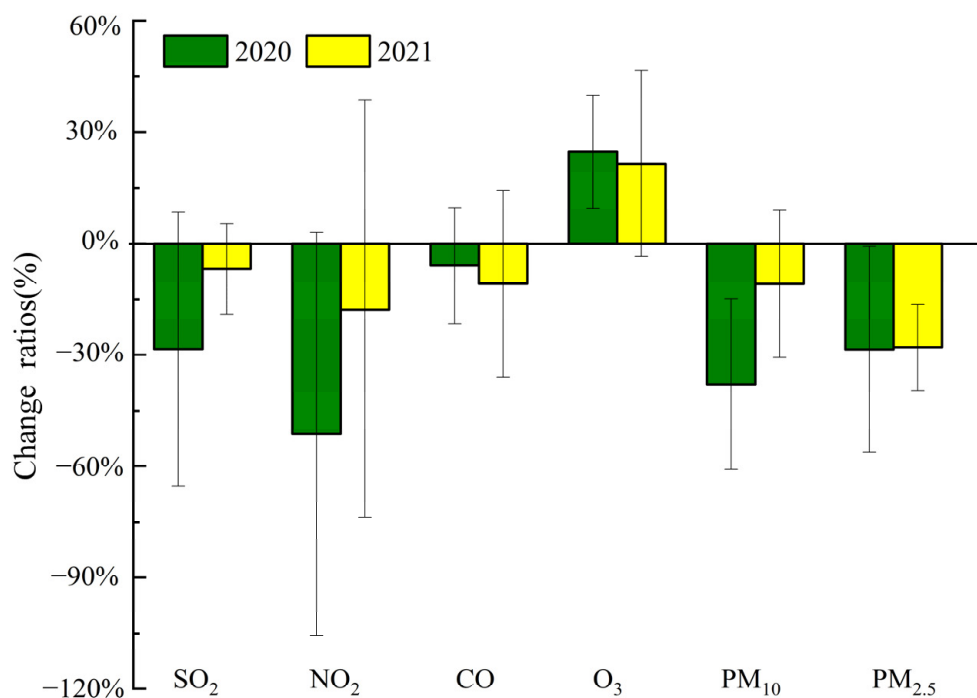


Figure 3. Change ratios of pollutant concentrations in 2020 and 2021 compared to 2019.

3.2. Chemical Compositions of PM_{2.5}

The concentration of secondary inorganic aerosols (SIAs) was 51.87 µg m⁻³ in 2019, 50.25 µg m⁻³ during the 2020 COVID-19 restrictions, and 45.21 µg m⁻³ in 2021. Compared with that in 2019, the SIA concentration decreased by 3.1% in 2020 and 12.8% in 2021. In contrast, the contributions of SIAs to PM_{2.5} increased from 50.61% in 2019 to 68.6% in 2020 and 61.2% in 2021. Between 2019 and 2021, SIAs were the major components of PM_{2.5}, with a greater impact in 2020 and 2021. Compared with that in 2019, the concentration of PM_{2.5} decreased by 29% during the 2020 COVID-19 restrictions and 28% in 2021, but the SIA concentration decreased by 3% and 13%, respectively. The different declines between PM_{2.5} and their SIAs may be attributed to NO₃⁻ and SO₄²⁻ formation.

The average concentrations of NO₃⁻, NH₄⁺, and SO₄²⁻ were 22.93 µg m⁻³, 13.69 µg m⁻³, and 15.25 µg m⁻³ in 2019 (Figure 4a). The average NO₃⁻ and NH₄⁺ concentrations were reduced by 9.8% and 5%, respectively, during the 2020 restriction period. In contrast, SO₄²⁻ increased by 8.6% in 2020. These results indicate that the reduction in precursor gases (NO_x and SO₂) did not result in proportionate reductions in NO₃⁻ and SO₄²⁻ during the 2020 restriction period compared to 2019. Mismatched decreases in NO₃⁻ levels with marked NO_x reductions and the puzzling SO₄²⁻ increase during the 2020 restriction period offset the decrease in PM_{2.5} levels in Zhengzhou. The average concentrations of NO₃⁻ in 2021 were similar to that in 2019. However, the average NH₄⁺ and SO₄²⁻ concentrations decreased by 16.9% and 28.9%, respectively, in 2021. The large reductions (18% and 58%) in NO₂ and NO also could not help alleviate NO₃⁻ formation in 2021, which was related to the high conversion rate of NO_x to nitrate (NOR). The restriction resulted in a decrease in PM_{2.5} levels; however, air quality remained episodically bad.

The average concentrations of OC and EC were 12.71 and 3.64 $\mu\text{g m}^{-3}$ in 2019, accounting for 12% and 4% of $\text{PM}_{2.5}$ mass (Figure 4b). The average concentrations of OC and EC were 8.97 and 2.76 $\mu\text{g m}^{-3}$ in 2020, 29% and 24% lower than those in 2019, respectively. In 2021, the average concentrations of OC and EC decreased by 38% and 15%, respectively. Although the average concentrations of OC and EC showed significant reductions in 2020 and 2021, the contributions to $\text{PM}_{2.5}$ were similar. The value of OC/EC was 4.31 (1.83~11.93) in 2019, 3.64 (1.99~9.71) in 2020, and 2.77 (1.16~8.74) in 2021. OC and EC are majorly emitted from fossil fuel combustion and biomass burning. Carbonaceous aerosols from biomass-burning sources have richer OC than EC, implying high OC/EC values. When OC/EC ratios were lower than 2.0, carbonaceous aerosols were from vehicular and industrial emissions. In addition, high OC/EC ratios (>2.0) indicate the presence of secondary organic aerosols (SOAs) [7,37,43]. OC/EC ratios mostly exceeded 2 in 2019 and 2021 (Figure S1), suggesting carbonaceous aerosols from biomass-burning sources. The mass concentration of SOA decreased from 10.31 $\mu\text{g m}^{-3}$ in 2019 to 5.83 $\mu\text{g m}^{-3}$ in 2020 and 6.88 $\mu\text{g m}^{-3}$ in 2021 (Figure 4 and Table 1). The reductions in SOA were 43.49% in 2020 and 33.21% in 2021. The changes in secondary inorganic species were much smaller than those in secondary organic aerosols.

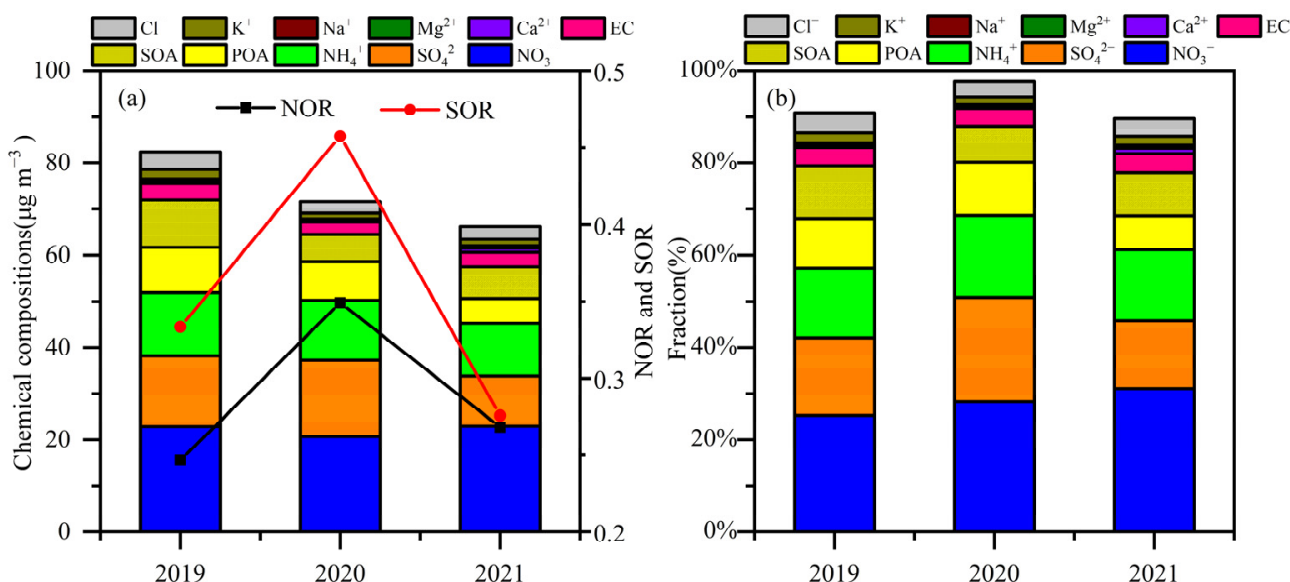


Figure 4. Average mass concentrations (a) and mass fractions (b) of $\text{PM}_{2.5}$ constituents (SO_4^{2-} , NO_3^- , NH_4^+ , POA, SOA, EC, Cl^- , K^+ , Na^+ , Mg^{2+} , and Ca^{2+}), NOR, and SOR in 2019, 2020, and 2021.

The average concentrations of Cl^- and K^+ decreased from 2.03 and 3.84 $\mu\text{g m}^{-3}$ in 2019 to 1.25 and 2.45 $\mu\text{g m}^{-3}$ in 2020 and to 1.47 and 2.79 $\mu\text{g m}^{-3}$ in 2021, implying a reduction in emissions from coal combustion and biomass burning in 2020 and 2021. The average concentrations of Ca^{2+} , Mg^{2+} , and Na^+ in 2019 were 0.46, 0.19, and 0.29 $\mu\text{g m}^{-3}$, respectively, which were 40%, 31%, and 26% higher than those in 2020 and 93%, -2%, and 7% lower than those in 2021.

3.3. Nitrate and Sulfate Formations over the Three Years

It is a puzzling phenomenon that SIA contributions to $\text{PM}_{2.5}$ were higher in 2020 (~68%) and in 2021 (~60%) than in 2019 (51%), when $\text{PM}_{2.5}$ decreased from 102.49 $\mu\text{g m}^{-3}$ (2019) to 73.92 $\mu\text{g m}^{-3}$ (2020) and 76.78 $\mu\text{g m}^{-3}$ (2021). SO_2 and NO_x are NO_3^- and SO_4^{2-} 's key precursor gases. To elucidate the puzzling phenomenon, the formation of NO_3^- and SO_4^{2-} was compared with their precursor gases, $\text{PM}_{2.5}$, and conversion ratios under different periods.

NO_3^- positively increased with NO_x between 2019 and 2021 (Figure 5 and Table S2, $p < 0.01$), indicating that high concentrations of the precursor contributed to high NO_3^-

levels and then led to the remarkable increases in $\text{PM}_{2.5}$. The result was supported by the positive relationship between NO_3^- and $\text{PM}_{2.5}$ (Table S2, $p < 0.01$). At a given precursor concentration, higher conversion ratios led to higher NO_3^- and SO_4^{2-} concentrations, implying that secondary conversion ratios were important for the formation of NO_3^- and SO_4^{2-} . It was found that NO_3^- and SO_4^{2-} levels were low in the region with high precursor gases region and low conversion ratios. The results suggested that the absolute concentrations of NO_3^- and SO_4^{2-} were more closely related to the secondary conversion rates than the precursor concentrations. A similar phenomenon was found in the summer of 2019 and 2020 [3].

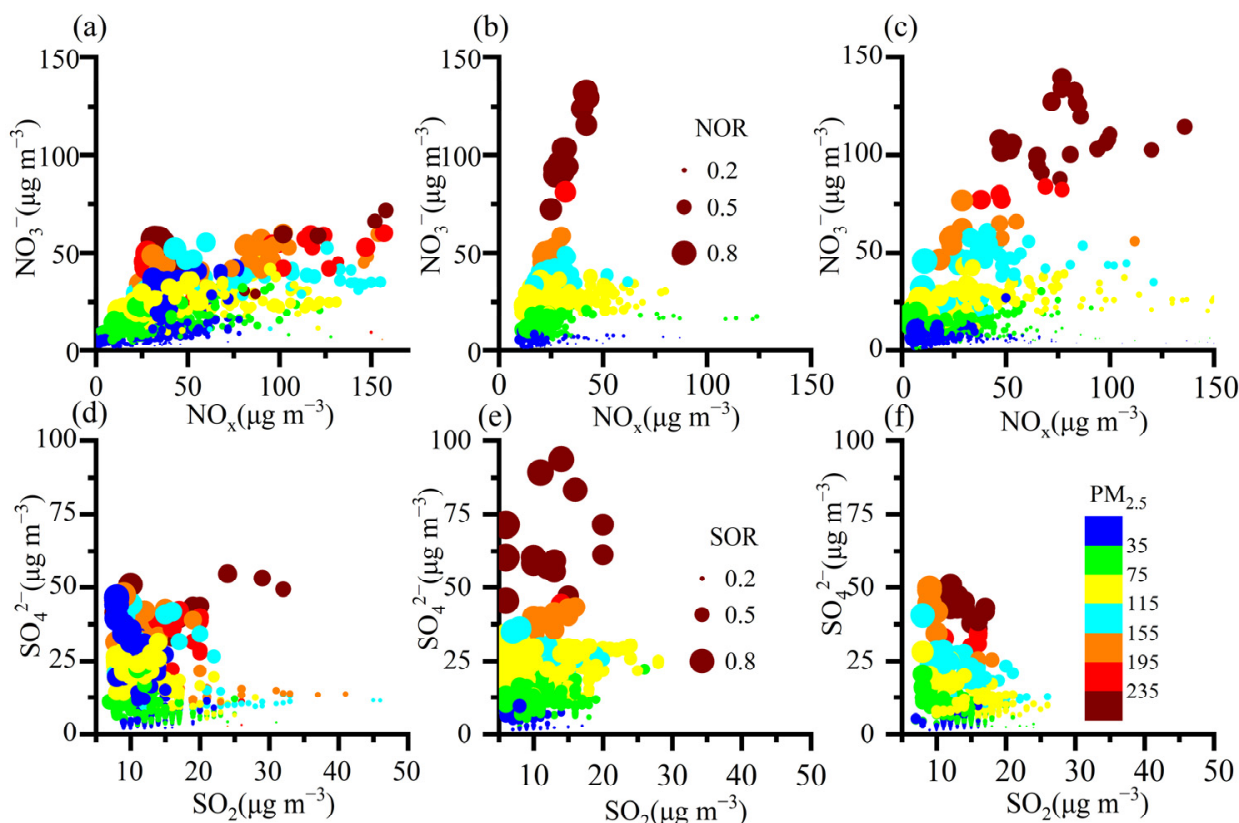


Figure 5. Correlations between NO_3^- , SO_4^{2-} , and precursor gases in 2019 (a,d), 2020 (b,e), and 2021 (c,f). Symbols in (a–f) are scaled by conversion ratios (NOR and SOR) and colored by $\text{PM}_{2.5}$ concentrations.

There were some exceptions in the same NO_x region when NO_3^- concentrations were higher in 2020 and 2021 than in 2019. In 2020 and 2021, the higher NO_3^- levels in the same NO_x region were closely related to the higher NOR. Meanwhile, in 2020, higher SO_4^{2-} concentrations in the same SO_2 region significantly correlated with higher SOR levels. It is equally inconceivable that higher conversion ratios occurred in 2020 and 2021 to cause high secondary formation, especially NO_3^- .

RH and O_3 are key factors regulating the oxidation pathways for nitrate and sulfate formation [14,15,37,45]. Both NOR and SOR were positively correlated with RH, as shown in Figure 6 and Table S4 ($p < 0.01$), suggesting that high RH favors the conversion of gaseous precursors (e.g., NO_x and SO_2) to NO_3^- and SO_4^{2-} . The NOR concentration was high in a high- O_3 region at a given RH, while the SOR was not (Figure 6). NOR was positively correlated with O_3 and O_3/O_x in 2019–2021 ($p < 0.01$, Table S4), but SOR was not. The results indicated that NO_x was efficiently oxidized by O_3 . O_3 increased in 2020 and 2021; higher NOR values were accompanied by higher O_3 and O_3/O_x values in a given RH, compared with 2019 (Figure 6), whereas the conversion rate of SO_2 to sulfate was not. O_3 was likely the major oxidant for the high level of NO_3^- formation.

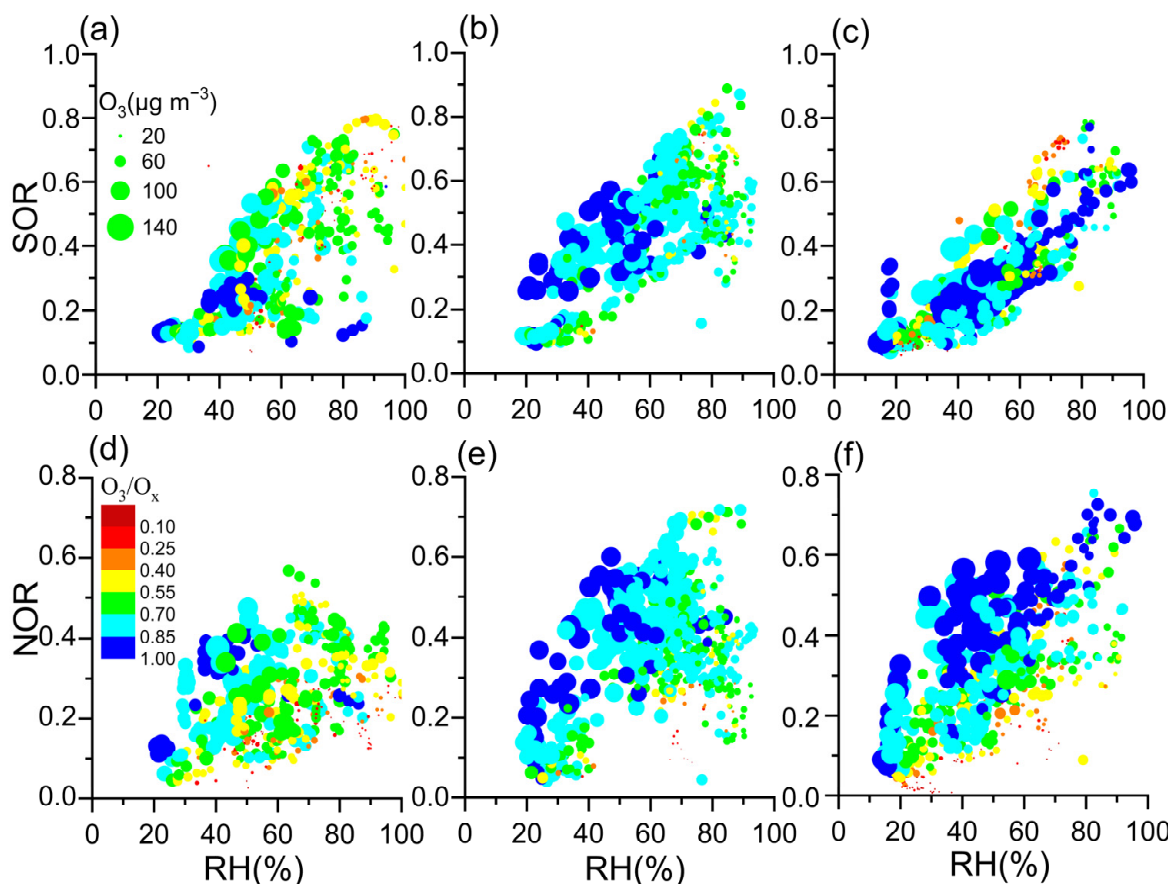


Figure 6. Correlations between conversion ratios (NOR and SOR) and RH in 2019 (a,d), 2020 (b,e), and 2021 (c,f). Symbols in (a–f) are scaled by O_3 concentration and colored by O_3/O_x . The oxidants (O_x) are the sum of NO_2 and O_3 , a proxy for atmospheric oxidation caused by photochemical reactions.

3.4. Sources during the Three Periods

The profiles of six factors were identified using the EPA PMF v5.0 in Figure 7. Factor 1 was characterized by the highly explained variations in Ni, Zn, Se, Mg^{2+} , Fe, and Mn in the three periods, identified as traffic emissions. Zn is widely used as an additive for lubricants in engines, vehicular tailpipe exhausts [45], debris from brake wear, and worn tires [46,47]. Factor 2 was dominated by high K^+ , Ba, and Mg^{2+} concentrations, generally indicators of biomass burning [48,49]. Factor 3 was characterized by highly explained variations in Ni, As, Cu, Ni, Mo, OC, and EC in 2019 and 2020, whereas Ba, As, OC, and EC in 2021 were identified as industrial emissions. This result was consistent with different industrial processes in the three areas. Studies have shown that steel sintering can emit large amounts of As, Zn, Ni, and Cu [21,50]. Factor 4 was dominated by high Cl^- , OC, and EC concentrations, generally indicators of coal combustion [21,40,51]. Factor 5 included large amounts of Mg^{2+} , Ca^{2+} , and Si [52–54]. Previous studies have shown that soil is also represented by a high loading of Ca, Mg, Si, and Al [47,49,54]; therefore, this factor was attributed to dust. Factor 6 was characterized by high NO_3^- , SO_4^{2-} , NH_4^+ , and OC content, as well as relatively high concentrations of OC. These species are mainly associated with secondary processes [46,50]. Thus, this factor was classified as a secondary aerosol.

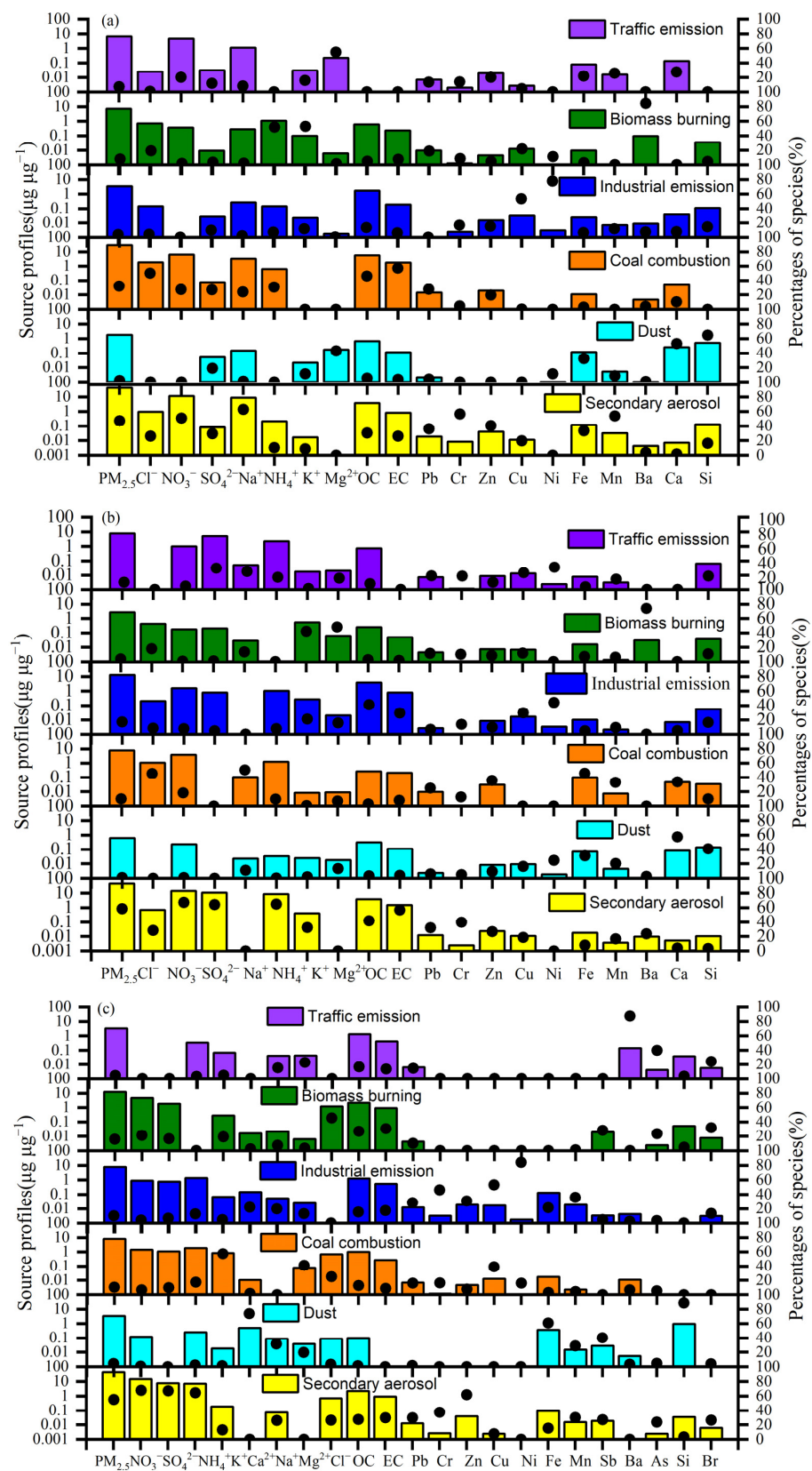


Figure 7. Six sources' profiles (bars) (in units of $\mu g \mu g^{-1}$) and contribution percentages (black dots) from each source factor resolved from the PMF model in 2019 (a), 2020 (b), and 2021 (c).

Secondary processes ($43.09 \mu\text{g m}^{-3}$), coal combustion ($29.18 \mu\text{g m}^{-3}$), biomass burning ($7.25 \mu\text{g m}^{-3}$), traffic emissions ($6.59 \mu\text{g m}^{-3}$), industrial emissions ($3.48 \mu\text{g m}^{-3}$), and dust ($1.87 \mu\text{g m}^{-3}$) were the six main sources of $\text{PM}_{2.5}$ in Zhengzhou in 2019, contributing 42.04%, 28.47%, 7.08%, 6.43%, 3.39%, and 1.82% of the $\text{PM}_{2.5}$, respectively (Table S5). Compared with 2019, the $\text{PM}_{2.5}$ mass concentration from the secondary aerosols in 2020 was similar to that in 2019, but the contribution of this source to $\text{PM}_{2.5}$ increased by 13.32%, which was consistent with the secondary inorganic components. In 2020, the $\text{PM}_{2.5}$ mass concentrations emitted by coal combustion, biomass burning, traffic emissions, industrial emissions, and dust showed obvious decreases. However, the contribution of coal combustion to $\text{PM}_{2.5}$ mass concentrations slightly increased by 2.87%, and the contributions of other sources to $\text{PM}_{2.5}$ mass concentrations slightly decreased by 0.41~3.27%. These results indicate that the changes in primary emissions from coal combustion, biomass burning, traffic emissions, industrial emissions, and dust were similar to those in the $\text{PM}_{2.5}$ level in 2020. The $\text{PM}_{2.5}$ mass concentrations from secondary aerosols, coal combustion, and traffic emissions in 2021 were lower than those in 2019, but the $\text{PM}_{2.5}$ mass concentrations emitted by industrial emissions and dust were higher. In 2021, the contribution of secondary aerosols to $\text{PM}_{2.5}$ levels was higher by 12.92% than that in 2019. However, coal combustion's contribution declined by 12.69%, suggesting that primary emissions from coal combustion were significantly reduced in 2021, while the influence of the secondary process on the $\text{PM}_{2.5}$ decreases was small. Secondary aerosols were the main source of $\text{PM}_{2.5}$ between 2019 and 2021, playing the more dominant role in $\text{PM}_{2.5}$ levels in 2020 and 2021 despite substantial reductions in gas emissions in 2020 and 2021. The primary emissions (biomass burning, traffic, and dust) were reduced by 29.71% in 2020 and 27.7% in 2021 compared to 2019. However, the $\text{PM}_{2.5}$ concentrations from the secondary processes in 2020 and 2021 were slightly decreased, and the contribution of the secondary processes to $\text{PM}_{2.5}$ increased by 13.32% in 2020 and 12.94% in 2021. The reductions in $\text{PM}_{2.5}$ levels in 2020 and 2021 were mainly due to a decline in primary emissions rather than the secondary process. A similar scenario, with higher contributions from secondary pollution to unexpected $\text{PM}_{2.5}$ levels, was found in many cities with COVID-19 restrictions [28,38,51–54].

4. Discussion

Significant improvements in air quality occurred during and after the COVID-19 outbreak in China, but haze still formed [1,2,13,34,41,55]. Many studies have found that enhancing secondary pollution inhibits these anomalies' continuous decline in $\text{PM}_{2.5}$ levels [9,32,38,56]. Changes in secondary aerosol formation under low precursor gas (NO_x and SO_2) levels with high O_3 levels throughout this pandemic remain unclear. Due to restrictions on residential and industrial activities implemented to prevent the spread of COVID-19 in Zhengzhou, $\text{PM}_{2.5}$ concentrations showed a remarkable decline of 29% during the 2020 COVID-19 restrictions compared with 2019. In addition, after the COVID-19 restrictions were lifted, $\text{PM}_{2.5}$ concentrations in 2021 were 28% lower than in 2019 (Figure 3). Moreover, the average molar concentration of total nitrogen compounds ($\text{NO}_x + \text{NO}_3^-$) in the air decreased from $1.60 \mu\text{mol m}^{-3}$ in 2019 to $0.89 \mu\text{mol m}^{-3}$ in 2020 and $1.44 \mu\text{mol m}^{-3}$ in 2021. Meanwhile, that of sulfur compounds ($\text{SO}_2 + \text{SO}_4^{2-}$) also slightly decreased from $0.39 \mu\text{mol m}^{-3}$ (2019) to $0.34 \mu\text{mol m}^{-3}$ (2020) and $0.33 \mu\text{mol m}^{-3}$ (2021), indicating that the reduction in nitrogen compounds during the 2020 COVID-19 restrictions was larger than that in 2021, while the decline in sulfur compounds was small. Ma et al. (2022) found that the average molar concentration of total nitrogen compounds before COVID-19 restrictions (January 1 to 23, 2020) was $2.74 \mu\text{mol m}^{-3}$, obviously higher than that during the COVID-19 restrictions; meanwhile, that of sulfur compounds ($0.36 \mu\text{mol m}^{-3}$) was slightly higher than that during the COVID-19 restrictions.

Despite significant decreases in total nitrogen in 2020 and 2021, NO_3^- levels were similar to that in 2019, while NO and NO_2 levels were significantly lower than that in 2019. This result indicates that nitrogen levels significantly changed when partitioning into NO_3^- , NO_2 , and NO in 2020 and 2021. It is a puzzle why a higher distribution of

NO_3^- occurred with lower NO and NO_2 in 2020 and 2021 than in 2019. It was found that the O_3 concentration was $1.21 \mu\text{mol m}^{-3}$ in 2020 and $1.18 \mu\text{mol m}^{-3}$ in 2021, higher than $0.97 \mu\text{mol m}^{-3}$ in 2019. O_3 molar concentrations in 2020 and 2021 were far greater than NO_2 molar concentrations ($0.47 \mu\text{mol m}^{-3}$ and $0.80 \mu\text{mol m}^{-3}$), respectively, implying that high O_3 promoted the conversion of NO to NO_2 , then to NO_3 , and finally to NO_3^- . Thus, NO levels in 2020 and 2021 were obviously lower than in 2019 (Table S1). The high production of NO_3^- from NO_x could have offset the effect of reduced total nitrogen on $\text{PM}_{2.5}$ levels [1,2].

NOR positively correlated with RH in 2019–2021 (Figure 6a,b and Table S4, $p < 0.01$). NOR was much higher in 2020 and 2021 than in 2019, when RH was higher than 40%. This result is consistent with high RH favoring NO_3^- formation via NO_x in 2020 and 2021 (Figure 6, Table S4). The increase in NOR with RH in the daytime was significantly higher than at nighttime (Figure 8). Moreover, the variations in NOR, O_3/O_x , and O_3 concentration were similar in the daytime (high) and nighttime (low) in 2019–2021 (Figure S4). Additionally, high O_3/O_x and O_3 concentrations in the daytime in 2020–2021 were accompanied by high NOR. In 2020 and 2021, high NOR meant high NO_3^- formation from NO_x . As shown in Figure 6, the high NOR was positively related to high O_3 and O_3/O_x (Table S4). The formation was likely because high O_3 promoted the conversion of NO to NO_2 , resulting in more NO_2 to form NO_3^- . If O_3 concentrations in 2020 and 2021 were similar to those in 2019, the NOR might have been similar to that (0.25) in 2019. NO_3^- concentrations in 2020 decreased from $20.36 \mu\text{g m}^{-3}$ to $11.44 \mu\text{g m}^{-3}$ in 2020, while NH_4^+ levels fell by $3.32 \mu\text{g m}^{-3}$. Thus, $\text{PM}_{2.5}$ levels decreased from 73.24 to $61.00 \mu\text{g m}^{-3}$ during the COVID-19 restriction period. Similarly, NO_3^- and NH_4^+ declined by $5.16 \mu\text{g m}^{-3}$ and $1.49 \mu\text{g m}^{-3}$ in 2021, resulting in a decrease ($\sim 7 \mu\text{g m}^{-3}$) in $\text{PM}_{2.5}$ levels. Enhanced NOR hindered a $\sim 17\%$ and $\sim 10\%$ decline in $\text{PM}_{2.5}$ levels during and after the COVID-19 restrictions in Zhengzhou. As a result of the increased O_3 , NO_3^- formation was enhanced by oxidizing NO to NO_2 , offsetting the reduction in $\text{PM}_{2.5}$ levels.

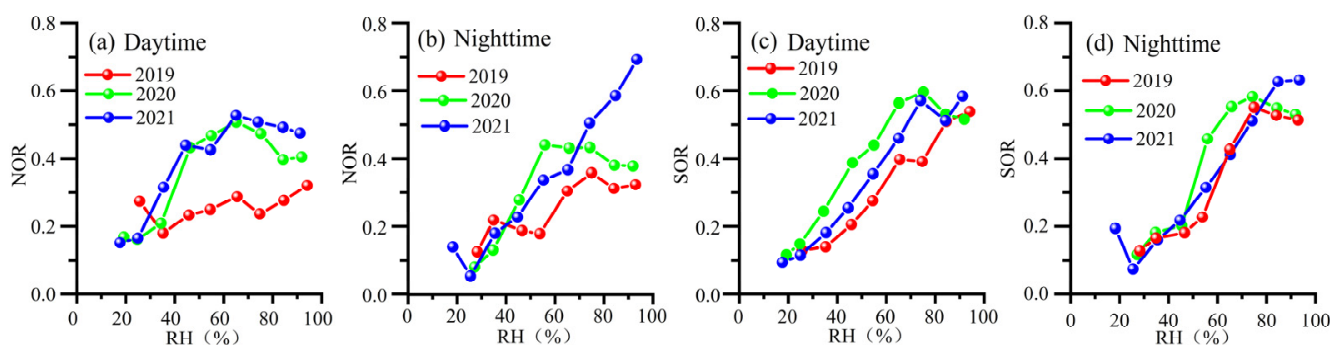


Figure 8. NOR and SOR with RH in the daytime (08:00–19:00) (a,c) and nighttime (20:00–07:00) (b,d) in 2019 2020 and 2021.

SOR increased with RH between 2019 and 2021 (Figure 6c,d). This result indicates that moist air favors the conversion of SO_2 to SO_4^{2-} . Moreover, the variation in SOR with RH was similar in the daytime and nighttime. O_3 concentration was high in the daytime and low at nighttime (Figures S4 and S5). On the contrary, SOR and RH levels were low in the daytime and high at nighttime. Figure 6a–c show that high SOR did not follow high O_3 levels under certain RH values between 2019 and 2021. Figure S3 and Table S4 depict the poor correlation between SOR and O_3 . The results suggest that photochemical reactions were not the major pathway of the SO_4^{2-} formation. Thus, the heterogeneous reactions on the particle surface were the major route for SO_4^{2-} formation, rather than photochemical reactions.

As shown in Figure S2, the slopes of NH_4^+ and $\text{NO}_3^- + 2 \text{SO}_4^{2-}$ were 1.11 in 2019, 1.02 in 2020, and 1.02 in 2021, implying that NH_4^+ was rich in 2019. The enhanced formation of

nitrate and sulfate in 2020 and 2021 may not have been caused by rich NH_4^+ . The wind speed was generally less than 2 m s^{-1} in 2019–2021 (Figure S6). Temperature has negative correlations with NO_3^- , SO_4^{2-} , and conversion ratios (NOR and SOR) (Tables S2–S4). The NO_3^- had similar levels in 2019–2021, despite lower total nitrogen compounds in 2020 and 2021 than in 2019. Thus, wind speed and temperature were not major factors for the enhanced NO_3^- . The normalized concentrations of NO_3^- by EC were to counteract the effect of the atmospheric physical processes and represent the contribution from chemical reactions [56] because EC was produced only from primary emissions and was a very inertial species to the chemical reactions. Its variability was mainly controlled by emission intensity and atmospheric physical processes. The NO_3^-/EC ratio increased from 6.30 in 2019 to 7.50 in 2020 and 7.44 in 2021, reflecting an elevated production of NO_3^- . The results were consistent with the variations in NO_3^- contributions to $\text{PM}_{2.5}$. An earlier study also observed a similar phenomenon [38,52–54]. Another earlier study reported that NOR increased from 0.14 to 0.21 in 2020 when Shanghai implemented restrictions [1]. In Xi'an, NOR increased from 0.33 in non-restriction periods to 0.57 in restriction periods, when O_3 concentration increased from 35.3 to $53.6 \mu\text{g m}^{-3}$ [38]. An investigation of the published data on haze occurrence during and after COVID-19 restrictions in many cities in China revealed a similar scenario, with photochemically enhanced NOR causing major contributions of NO_3^- to $\text{PM}_{2.5}$ and inhibiting the continuous decline in $\text{PM}_{2.5}$ levels [1,9,25,38].

5. Conclusions

Despite significant improvements in air quality during and after COVID-19 restrictions, due to strict regulations on residential and industrial activities to curb the spread of COVID-19, haze still occurred in Zhengzhou. The average concentration of $\text{PM}_{2.5}$ decreased from $102.49 \mu\text{g m}^{-3}$ before the restrictions (2019) to $73.24 \mu\text{g m}^{-3}$ during the restrictions (2020) and $73.90 \mu\text{g m}^{-3}$ after the restrictions (2021). In 2019, SIA concentrations declined by 3.1% in 2020 and 12.8% in 2021. At the same time, the contributions of SIAs to $\text{PM}_{2.5}$ increased to 68.6% (2020) and 61.2% (2021), higher than 50.61% in 2019. SIAs caused major contributions to $\text{PM}_{2.5}$ levels in 2020 and 2021. NO_x levels in 2020 and 2021 were 22–62% lower than that in 2019; however, NO_3^- concentrations had similar levels (20.69 – $23.00 \mu\text{g m}^{-3}$) in 2019, 2020, and 2021, which was attributed to the enhanced conversion rate of NO_x to nitrate by the increased O_3 levels in 2020 and 2021. The inconsistent reduction between nitrate and NO_x inhibited further $\text{PM}_{2.5}$ reduction and contributed to haze formation in Zhengzhou.

Six of the $\text{PM}_{2.5}$ sources were secondary inorganic aerosols, industrial emissions, coal combustion, biomass burning, soil dust, and traffic emissions in 2019, 2020, and 2021. Compared with 2019, the primary emissions (biomass burning, traffic, and dust) were reduced by 29.71% in 2020 and 27.7% in 2021. However, the $\text{PM}_{2.5}$ from the secondary process in 2020 and 2021 decreased slightly, and the contribution of the secondary process to $\text{PM}_{2.5}$ increased by 12.94%–13.32% in 2020 and 2021. The reductions in $\text{PM}_{2.5}$ levels in 2020 and 2021 were mainly due to a decline in primary emissions rather than the secondary process. Thus, a better understanding of the formation of secondary aerosols under high O_3 and low precursor gases would be needed to help mitigate air pollution in the future.

Supplementary Materials: The following supporting information can be downloaded at: <https://www.mdpi.com/article/10.3390/toxics12010081/s1>. Figure S1: The OC/EC ratios in 2019 (a), 2020 (b) and 2021 (c); Figure S2: NOR and SOR with O_3 in 2019, 2020 and 2021; Figure S3: NOR and SOR with O_3 in 2019, 2020 and 2021; Figure S4: The diurnal variations of NOR and SOR in 2019 (a), 2020 (b) and 2021 (c); Figure S5: The diurnal variations of RH, O_3 and O_3/O_x in 2019 (a), 2020 (b) and 2021 (c); Figure S6: Statistical analysis of wind speed in 2019–2021; Table S1: Average mass concentrations ($\mu\text{g m}^{-3}$) of air pollutants and species in $\text{PM}_{2.5}$ in 2019, 2020 and 2021; Table S2: Correlation analysis between NO_3^- , $\text{PM}_{2.5}$, T, RH and NOR in 2019–2021 (Pearson correlation coefficients); Table S3: Correlation analysis between SO_4^{2-} , $\text{PM}_{2.5}$, T, RH and SOR in 2019–2021 (Pearson correlation coefficients); Table S4: Correlation analysis between conversion ratios (NOR and SOR), RH, O_3 and O_3/O_x in 2019–2021 (Pearson correlation coefficients); Table S5: Average contributions (%) of six sources to $\text{PM}_{2.5}$ in 2019, 2020 and 2021.

Author Contributions: Conceptualization, Q.M. and K.H.; methodology, W.W.; software, A.C. and K.H.; validation, S.Z. and J.H.; formal analysis, A.C. and Q.M.; data curation, Q.M.; writing—original draft preparation, S.Z. and Q.M.; writing—review and editing, J.H., K.H.; and Q.M. All authors have read and agreed to the published version of the manuscript.

Funding: This research was funded by the Natural Science Foundation of China (42105071) and the project of science and technology of the Henan province for tackling key problems (212102110390).

Institutional Review Board Statement: Not applicable.

Informed Consent Statement: Not applicable.

Data Availability Statement: The data presented in this study are available on request from the corresponding author.

Conflicts of Interest: The authors declare no conflict of interest.

References

1. Chang, Y.; Huang, R.-J.; Ge, X.; Huang, X.; Hu, J.; Duan, Y.; Zou, Z.; Liu, X.; Lehmann, M. Puzzling haze events in China during the coronavirus (COVID-19) shutdown. *Geophys. Res. Lett.* **2020**, *47*, e2020GL088533. [[CrossRef](#)]
2. Le, T.H.; Wang, Y.; Liu, L.; Yang, J.N.; Yung, Y.L.; Li, G.H.; Seinfeld, J.H. Unexpected air pollution with marked emission reductions during the COVID-19 outbreak in China. *Science* **2020**, *369*, 702. [[CrossRef](#)] [[PubMed](#)]
3. Li, R.; Zhao, Y.L.; Fu, H.B.; Chen, J.M.; Peng, M.; Wang, C.Y. Substantial changes in gaseous pollutants and chemical compositions in fine particles in the North China Plain during the COVID-19 lockdown period: Anthropogenic vs. meteorological influences. *Atmos. Chem. Phys.* **2021**, *21*, 8677–8692. [[CrossRef](#)]
4. Pei, Z.; Han, G.; Ma, X.; Su, H.; Gong, W. Response of major air pollutants to COVID-19 lockdowns in China. *Sci. Total Environ.* **2020**, *743*, 140879. [[CrossRef](#)]
5. Shi, X.Q.; Brasseur, G.P. The response in air quality to the reduction of Chinese economic activities during the COVID-19 outbreak. *Geophys. Res. Lett.* **2020**, *47*, e2020GL088070. [[CrossRef](#)] [[PubMed](#)]
6. Wang, Y.C.; Wu, R.; Liu, L.; Yuan, Y.; Liu, C.G.; Ho, S.S.H.; Ren, H.H.; Wang, Q.Y.; Lv, Y.; Yan, M.Y.; et al. Differential health and economic impacts from the COVID-19 lockdown between the developed and developing countries: Perspective on air pollution. *Environ. Pollut.* **2022**, *293*, 118544. [[CrossRef](#)]
7. Chen, H.; Huo, J.; Fu, Q.; Duan, Y.; Xiao, H.; Chen, J. Impact of quarantine measures on chemical compositions of PM_{2.5} during the COVID-19 epidemic in Shanghai, China. *Sci. Total Environ.* **2020**, *743*, 140758. [[CrossRef](#)]
8. Huang, G.Y.; Sun, K. Non-negligible impacts of clean air regulations on the reduction of tropospheric NO₂ over East China during the COVID-19 pandemic observed by OMI and TROPOMI. *Sci. Total Environ.* **2020**, *745*, 141023. [[CrossRef](#)]
9. Sun, Y.; Lei, L.; Zhou, W.; Chen, C.; He, Y.; Sun, J.; Li, Z.; Xu, W.; Wang, Q.; Ji, D.; et al. A Chemical Cocktail during the COVID-19 Outbreak in Beijing, China: Insights from Six-Year Aerosol Particle Composition Measurements during the Chinese New Year Holiday. *Sci. Total Environ.* **2020**, *742*, 140739. [[CrossRef](#)]
10. Xie, X.D.; Hu, J.L.; Qin, M.M.; Guo, S.; Hu, M.; Ji, D.S.; Wang, H.L.; Lou, S.R.; Huang, C.; Liu, C.; et al. Particle Phase State and Aerosol Liquid Water Greatly Impact Secondary Aerosol Formation: Insights into Phase Transition and Role in Haze Events. *Atmos. Chem. Phys.* **2023**, *23*, 10563–10578. [[CrossRef](#)]
11. Gen, M.S.; Zhang, R.F.; Huang, D.D.; Li, Y.J.; Chan, C.K. Heterogeneous Oxidation of SO₂ in Sulfate Production during Nitrate Photolysis at 300 nm: Effect of pH, Relative Humidity, Irradiation Intensity, and the Presence of Organic Compounds. *Environ. Sci. Technol.* **2019**, *53*, 8757–8766. [[CrossRef](#)] [[PubMed](#)]
12. Li, X.; Zhao, B.; Zhou, W.; Shi, H.; Yin, R.; Cai, R.; Yang, D.; Dallenbach, K.; Deng, C.; Fu, Y.; et al. Responses of gaseous sulfuric acid and particulate sulfate to reduced SO₂ concentration: A perspective from long-term measurements in Beijing. *Sci. Total Environ.* **2020**, *721*, 137700. [[CrossRef](#)] [[PubMed](#)]
13. Ma, Q.X.; Wang, W.S.; Wu, Y.F.; Wang, F.; Jin, L.Y.; Song, X.Y.; Han, Y.; Zhang, R.J.; Zhang, D.Z. Haze caused by NO_x oxidation under restricted residential and industrial activities in a mega city in the south of North China Plain. *Chemosphere* **2022**, *305*, 135489. [[CrossRef](#)] [[PubMed](#)]
14. Peng, J.F.; Hu, M.; Shang, D.J. Explosive Secondary Aerosol Formation during Severe Haze in the North China Plain. *Environ. Sci. Technol.* **2021**, *55*, 2189–2207. [[CrossRef](#)] [[PubMed](#)]
15. Fang, Y.; Ye, C.; Wang, J.; Wu, Y.; Hu, M.; Lin, W.; Xu, F.; Zhu, T. Relative humidity and O₃ concentration as two prerequisites for sulfate formation. *Atmos. Chem. Phys.* **2019**, *19*, 12295–12307. [[CrossRef](#)]
16. Liu, T.; Clegg, S.L.; Abbatt, J.P.D. Fast oxidation of sulfur dioxide by hydrogen peroxide in deliquesced aerosol particles. *Proc. Natl. Acad. Sci. USA* **2020**, *117*, 1354–1359. [[CrossRef](#)]
17. Pandis, S.N.; Seinfeld, J.H.; Pilinis, C. Heterogeneous sulfate production in an urban fog. *Atmos. Environ. Part A-Gen. Top.* **1992**, *26*, 2509–2522. [[CrossRef](#)]
18. Ding, J.; Dai, Q.L.; Zhang, Y.F.; Xu, J.; Huangfu, Y.Q.; Feng, Y.C. Air humidity affects secondary aerosol formation in different pathways. *Sci. Total Environ.* **2021**, *759*, 143540. [[CrossRef](#)]

19. Li, G.; Bei, N.; Cao, J.; Huang, R.; Wu, J.; Feng, T.; Wang, Y.; Liu, S.; Zhang, Q.; Tie, X.; et al. A possible pathway for rapid growth of sulfate during haze days in China. *Atmos. Chem. Phys.* **2017**, *17*, 3301–3316. [[CrossRef](#)]
20. Ma, Q.X.; Wu, Y.F.; Zhang, D.Z.; Wang, X.J.; Xia, Y.J.; Liu, X.Y.; Tian, P.; Han, Z.W.; Xia, X.A.; Wang, Y.; et al. Roles of regional transport and heterogeneous reactions in the PM_{2.5} increase during winter haze episodes in Beijing. *Sci. Total Environ.* **2017**, *599–600*, 246–253. [[CrossRef](#)]
21. Cheng, Y.F.; Zheng, G.J.; Wei, C.; Mu, Q.; Zheng, B.; Wang, Z.B.; Gao, M.; Zhang, Q.; He, K.B.; Carmichael, G.; et al. Reactive nitrogen chemistry in aerosol water as a source of sulfate during haze events in China. *Sci. Adv.* **2016**, *2*, 11. [[CrossRef](#)]
22. George, C.; Ammann, M.; D’Anna, B.; Donaldson, D.J.; Nizkorodov, S.A. Heterogeneous photochemistry in the atmosphere. *Chem. Rev.* **2015**, *115*, 4218–4258. [[CrossRef](#)] [[PubMed](#)]
23. Fu, X.; Wang, T.; Gao, J.; Wang, P.; Liu, Y.; Wang, S.; Zhao, B.; Xue, L. Persistent heavy winter nitrate pollution driven by increased photochemical oxidants in northern China. *Environ. Sci. Technol.* **2020**, *54*, 3881–3889. [[CrossRef](#)] [[PubMed](#)]
24. Li, H.; Ma, Y.L.; Duan, F.K.; Zhu, L.D.; Ma, T.; Yang, S.; Xu, Y.Z.; Li, F.; Huang, T.; Kimoto, T.; et al. Stronger secondary pollution processes despite decrease in gaseous precursors: A comparative analysis of summer 2020 and 2019 in Beijing. *Environ. Pollut.* **2021**, *279*, 116923. [[CrossRef](#)] [[PubMed](#)]
25. Liu, P.F.; Ye, C.; Xue, C.Y.; Zhang, C.L.; Mu, Y.J.; Sun, X. Formation mechanisms of atmospheric nitrate and sulfate during the winter haze pollution periods in Beijing: Gas–phase, heterogeneous and aqueous–phase chemistry. *Atmos. Chem. Phys.* **2020**, *20*, 4153–4165. [[CrossRef](#)]
26. Khoder, M.I. Atmospheric conversion of sulfur dioxide to particulate sulfate and nitrogen dioxide to particulate nitrate and gaseous nitric acid in an urban area. *Chemosphere* **2002**, *49*, 675–684. [[CrossRef](#)]
27. Wang, G.H.; Zhang, R.Y.; Gomez, M.E. Persistent sulfate formation from London fog to Chinese haze. *Proc. Natl. Acad. Sci. USA* **2016**, *113*, 13630–13635. [[CrossRef](#)]
28. Lin, Y.C.; Zhang, Y.L.; Fan, M.Y.; Bao, M.Y. Heterogeneous formation of particulate nitrate under ammonium-rich regimes during the high-PM_{2.5} events in Nanjing, China. *Atmos. Chem. Phys.* **2020**, *20*, 3999–4011. [[CrossRef](#)]
29. Fan, C.; Li, Y.; Guang, J.; Li, Z.; Elnashar, A.; Allam, M.; de Leeuw, G. The impact of the control measures during the COVID-19 outbreak on air pollution in China. *Remote Sens.* **2020**, *12*, 1613. [[CrossRef](#)]
30. Feng, S.Z.; Jiang, F.; Wang, H.M.; Wang, H.K.; Ju, W.M.; Shen, Y.; Zheng, Y.H.; Wu, Z.; Ding, A.J. NO_x emission changes over China during the COVID-19 epidemic inferred from surface NO₂ observations. *Geophys. Res. Lett.* **2020**, *47*, e2020GL090080. [[CrossRef](#)]
31. Liang, Y.X.; Gui, K.; Che, H.Z.; Li, L.; Zheng, Y.; Zhang, X.T.; Zhang, X.D.; Zhang, P.; Zhang, X.Y. Changes in aerosol loading before, during and after the COVID-19 pandemic outbreak in China: Effects of anthropogenic and natural aerosol. *Sci. Total Environ.* **2023**, *857*, 159435. [[CrossRef](#)]
32. Tian, J.; Wang, Q.Y.; Zhang, Y.; Yan, M.Y.; Liu, H.K.; Zhang, N.N.; Ran, W.K.; Cao, J.J. Impacts of primary emissions and secondary aerosol formation on air pollution in an urban area of China during the COVID-19 lockdown. *Environ. Inter.* **2021**, *150*, 106426. [[CrossRef](#)]
33. Zhang, Q.Q.; Pan, Y.P.; He, Y.X.; Walters, W.W.; Ni, Q.Y.; Liu, X.Y.; Xu, G.Y.; Shao, J.L.; Jiang, C.L. Substantial nitrogen oxides emission reduction from China due to COVID-19 and its impact on surface ozone and aerosol pollution. *Sci. Total Environ.* **2021**, *753*, 142238. [[CrossRef](#)]
34. Lian, X.B.; Huang, J.P.; Huang, R.J.; Liu, C.W.; Wang, L.N.; Zhang, T.H. Impact of city lockdown on the air quality of COVID-19-hit of Wuhan city. *Sci. Total Environ.* **2020**, *742*, 140556. [[CrossRef](#)] [[PubMed](#)]
35. Liu, L.; Zhang, J.; Du, R.G.; Teng, X.M.; Hu, R.; Yuan, Q.; Tang, S.S.; Ren, C.H.; Huang, X.; Xu, L.; et al. Chemistry of Atmospheric Fine Particles during the COVID-19 Pandemic in a Megacity of Eastern China. *Geophys. Res. Lett.* **2021**, *48*, e2020GL091611. [[CrossRef](#)] [[PubMed](#)]
36. Wang, J.F.; Li, J.Y.; Ye, J.H.; Zhao, Y.; Wu, J.Z.; Hu, J.L.; Liu, D.T.; Nie, D.Y.; Shen, F.Z.; Huang, X.P.; et al. Fast sulfate formation from oxidation of SO₂ by NO₂ and HONO observed in Beijing haze. *Nat. Commun.* **2020**, *11*, 2844. [[CrossRef](#)] [[PubMed](#)]
37. Chang, X.; Zheng, H.T.; Zhao, B.; Yan, C.; Jiang, Y.Q.; Hu, R.L.; Song, A.J.; Dong, Z.X.; Li, S.Y.; Li, Z.Q.; et al. Drivers of High Concentrations of Secondary Organic Aerosols in Northern China during the COVID-19 Lockdowns. *Environ. Sci. Technol.* **2023**, *57*, 5521–5531. [[CrossRef](#)]
38. Duan, J.; Huang, R.J.; Chang, Y.H. Measurement report of the change of PM_{2.5} composition during the COVID-19 lockdown in urban Xi’an: Enhanced secondary formation and oxidation. *Sci. Total Environ.* **2021**, *791*, 148126. [[CrossRef](#)]
39. Li, Y.; Han, Z.W.; Song, Y.; Li, J.W.; Sun, Y.L.; Wang, T.T. Impacts of the COVID-19 lockdown on atmospheric oxidizing capacity and secondary aerosol formation over the Beijing-Tianjin-Hebei region in Winter-Spring 2020. *Atmos. Environ.* **2023**, *295*, 119540. [[CrossRef](#)]
40. Du, H.Y.; Li, J.; Wang, Z.F.; Yang, W.Y.; Chen, X.S.; Wei, Y. Sources of PM_{2.5} and its responses to emission reduction strategies in the Central Plains Economic Region in China: Implications for the impacts of COVID-19. *Environ. Pollut.* **2021**, *288*, 117783. [[CrossRef](#)]
41. Yang, J.R.; Wang, S.B.; Zhang, R.Q.; Yin, S.S. Elevated particle acidity enhanced the sulfate formation during the COVID-19 pandemic in Zhengzhou, China. *Environ. Pollut.* **2022**, *296*, 118716. [[CrossRef](#)] [[PubMed](#)]
42. Chen, X.; Walker, J.T.; Geron, C. Chromatography related performance of the Monitor for Aerosols and Gases in ambient air (MARGA): Laboratory and field-based evaluation. *Atmos. Meas. Tech.* **2017**, *10*, 3893–3908. [[CrossRef](#)]

43. Stieger, B.; Spindler, G.; Fahlbusch, B.; Müller, K.; Grüner, A.; Poulain, L.; Thöni, L.; Seitzler, E.; Wallasch, M.; Herrmann, H. Measurements of PM₁₀ ions and trace gases with the online system MARGA at the research station Melpitz in Germany—A five-year study. *J. Atmos. Chem.* **2018**, *75*, 33–70. [[CrossRef](#)]
44. Wu, C.; Wu, D.; Yu, J.Z. Estimation and Uncertainty Analysis of Secondary Organic Carbon Using 1 Year of Hourly Organic and Elemental Carbon Data. *J. Geophys. Res. Atmos.* **2019**, *124*, 2774–2795. [[CrossRef](#)]
45. Li, Z.Y.; Liu, J.J.; Zhai, Z.; Liu, C.; Ren, Z.Z.; Yue, Z.Y.; Yang, D.Y.; Hu, Y.; Zheng, H.; Kong, S.F. Heterogeneous changes of chemical compositions, sources and health risks of PM_{2.5} with the “Clean Heating” policy at urban/suburban/industrial sites. *Sci. Total Environ.* **2023**, *854*, 158871. [[CrossRef](#)]
46. Zhou, H.J.; Liu, T.; Sun, B.; Tian, Y.L.; Zhou Xj Hao, F.; Chun, X.; Wan, Z.Q.; Liu, P.; Wang, J.W.; Du, D.L. Chemical characteristics and sources of PM_{2.5} in Hohhot, a semi-arid city in northern China: Insight from the COVID-19 lockdown. *Atmos. Chem. Phys.* **2022**, *22*, 12153–12166. [[CrossRef](#)]
47. Hao, Q.; Jiang, N.; Zhang, R.Q.; Yang, L.M.; Li, S.L. Characteristics, sources, and reactions of nitrous acid during winter at an urban site in the Central Plains Economic Region in China. *Atmos. Chem. Phys.* **2020**, *20*, 7087–7102. [[CrossRef](#)]
48. Zhang, R.J.; Jing, J.; Tao, J.; Hsu, S.-C.; Wang, G.; Cao, J.; Lee, C.S.L.; Zhu, L.; Chen, Z.; Zhao, Y.; et al. Chemical characterization and source apportionment of PM_{2.5} in Beijing: Seasonal perspective. *Atmos. Chem. Phys.* **2013**, *13*, 7053–7074. [[CrossRef](#)]
49. Cui, Y.; Ji, D.S.; Maenhaut, W.; Gao, W.K.; Zhang, R.J.; Wang, Y.S. Levels and sources of hourly PM_{2.5}-related elements during the control period of the COVID-19 pandemic at a rural site between Beijing and Tianjin. *Sci. Total Environ.* **2020**, *744*, 140840. [[CrossRef](#)]
50. Zheng, H.; Kong, S.; Chen, N.; Yan, Y.; Liu, D.; Zhu, B.; Xu, K.; Cao, W.; Ding, Q.; Lan, B.; et al. Significant changes in the chemical compositions and sources of PM_{2.5} in Wuhan since the city lockdown as COVID-19. *Sci. Total Environ.* **2020**, *739*, 140000. [[CrossRef](#)]
51. Liu, H.; Tian, H.; Zhang, K.; Liu, S.; Cheng, K.; Yin, S.; Liu, Y.; Liu, X.; Wu, Y.; Liu, W.; et al. Seasonal variation, formation mechanisms and potential sources of PM_{2.5} in two typical cities in the Central Plains Urban Agglomeration, China. *Sci. Total Environ.* **2019**, *657*, 657–670. [[CrossRef](#)] [[PubMed](#)]
52. Kong, S.F.; Li, L.; Li, X.X.; Yin, Y.; Chen, K.; Liu, D.T.; Yuan, L.; Zhang, Y.J.; Shan, Y.P.; Ji, Y.Q. The impacts of firework burning at the Chinese Spring Festival on air quality: Insights of tracers, source evolution and aging processes. *Atmos. Chem. Phys.* **2015**, *15*, 2167–2184. [[CrossRef](#)]
53. Tian, Y.; Zhang, Y.; Liang, Y.; Niu, Z.; Xue, Q.; Feng, Y. PM_{2.5} source apportionment during severe haze episodes in a Chinese megacity based on a 5-month period by using hourly species measurements: Explore how to better conduct PMF during haze episodes. *Atmos. Environ.* **2020**, *224*, 117364. [[CrossRef](#)]
54. Hong, Y.; Xu, X.; Liao, D.; Zheng, R.; Ji, X.; Chen, Y.; Xu, L.; Li, M.; Wang, H.; Xiao, H.; et al. Source apportionment of PM_{2.5} and sulfate formation during the COVID-19 lockdown in a coastal city of southeast China. *Environ. Pollut.* **2021**, *286*, 117577. [[CrossRef](#)] [[PubMed](#)]
55. Huang, X.; Ding, A.; Gao, J.; Zheng, B.; Zhou, D.; Qi, X.; Tang, R.; Wang, J.; Ren, C.; Nie, W.; et al. Enhanced secondary pollution offset reduction of primary emissions during COVID-19 lockdown in China. *Natl. Sci. Rev.* **2020**, *8*, nwa137. [[CrossRef](#)]
56. Ma, Q.X.; Wu, Y.F.; Fu, S.L.; Zhang, D.Z.; Han, Z.W.; Zhang, R.J. Pollution severity-dependent aerosol light scattering enhanced by inorganic species formation in Beijing haze. *Sci. Total Environ.* **2020**, *719*, 137545. [[CrossRef](#)]

Disclaimer/Publisher’s Note: The statements, opinions and data contained in all publications are solely those of the individual author(s) and contributor(s) and not of MDPI and/or the editor(s). MDPI and/or the editor(s) disclaim responsibility for any injury to people or property resulting from any ideas, methods, instructions or products referred to in the content.